Gas Transport in Poly(vinylidene Fluoride): Effects of Uniaxial Drawing and Processing Temperature

M. J. EL-HIBRI and D. R. PAUL, *Department of Chemical Engineering and Center for Polymer Research, University of Texas, Austin, Texas 78712*

Synopsis

This paper reports on the gas sorption and transport properties of poly(vinylidene fluoride) (PVF_2) and on the effects uniaxial drawing and processing temperature have on these properties. Sorption and transport were first examined for "as-received" commercial Kynar PVF_2 film at 35°C. This film was 54% crystalline by weight. Solubility, diffusion, and permeability coefficients were measured for He, H_2, Ar, O_2, N_2, CH_4, and CO_2. The solubility coefficient and the diffusion coefficient D were correlated with the Lennard–Jones potential and mean molecular diameter of the gas, respectively. Uniaxial drawing of PVF_2 films was performed up to a draw ratio of 3.7 and over the temperature range 75–140°C. Transport properties were correlated with the extent of draw and drawing temperature. The permeability P and D were found to significantly decline with uniaxial drawing; the magnitude of this effect was dependent on both the drawing temperature and the molecular size of the penetrant considered. Reductions in P and D became progressively more pronounced with increasing molecular diameter and with decreasing drawing temperature (down to a limit of about 75°C), which reflects an increase in effectiveness of drawing at low temperatures. PVF_2 films annealed above 75°C showed an increase in P and D as opposed to the effect of drawing. The solubility of various gases in PVF_2 was not found to be sensitive to processing treatments such as drawing and annealing, in agreement with the relatively small changes observed in free volume. PVF_2 films subjected to various treatments were characterized by DSC, density, birefringence, and dynamic mechanical measurements. Gas transport measurements appear to provide a more sensitive and hence more viable measure of the effectiveness of drawing than these other techniques. Drawing PVF_2 in the melt state was found to increase P and D, in contrast with the effects observed for solid-state drawing. The results have been interpreted in terms of existing theories on morphology and microstructure in semicrystalline polymers.

INTRODUCTION

In an earlier paper[1] we reported a detailed study of the gas sorption and transport behavior of poly(vinyl chloride), a glassy and primarily amorphous material, and how these characteristics are influenced by uniaxial drawing and heat treatment. The latter processing steps were found to have substantial effects on the transport properties of PVC. In the present work, we focus on the effects of drawing and thermal treatments on gas transport in poly(vinylidene fluoride) (PVF_2), which is a semicrystalline polymer whose amorphous fraction is rubbery at room temperature.

PVF_2 is a good barrier material, having gas permeabilities of the same order as those for PVC, and has excellent chemical resistance. PVF_2 is now finding some commercial uses in miscible blends with poly(methyl methacrylate) for applications requiring good barrier performance and resistance to harsh chemical environments. These factors prompted us to examine the effects of uniaxially drawing PVF_2 over a wide range of temperatures on

Journal of Applied Polymer Science, Vol. 31, 2533–2560 (1986)
 CCC 0021-8995/86/082533-28$04.00

the gas transport behavior of this polymer. As background for this investigation, a detailed study was made of the gas sorption and permeation characteristics of an as-received commercial PVF_2 film.

Treated films were characterized by means of density, birefringence, differential scanning calorimetry and dynamic mechanical testing, and the gas transport results have been interpreted in terms of these characterization measurements.

BACKGROUND

Sorption of gases in rubbery noncrystalline polymers is well-described by Henry's Law

$$C = k^*p \tag{1}$$

which defines a solubility coefficient k* relating the equilibrium concentration of gas to the pressure. If the polymer is semicrystalline, gas dissolves exclusively in the amorphous regions, and eq. (1) becomes

$$C = k^*\alpha p = kp \tag{2}$$

where α is the amorphous volume fraction of the polymer. Thus, the overall solubility coefficient k for the material is given by

$$k = k^*\alpha \tag{3}$$

Also, for such polymers, the permeability P is related to the solubility coefficient and the diffusion coefficient D by

$$P = kD \tag{4}$$

where D can be estimated from the diffusion time lag θ and membrane thickness l using the simple expression

$$D = l^2/6\theta \tag{5}$$

Thus, eqs. (4) and (5) together provide an alternate method for determining the solubility from the experimental measurement of P and D. The solubility coefficient computed from transient permeation measurements is designated here by k_t to distinguish it from the solubility obtained by direct equilibrium measurement k.

When the polymer possesses crystallinity, the diffusion coefficient D is also reduced relative to that of the same material in a purely amorphous state. The reduction in D is the result of the impermeable nature of the dispersed crystalline phase, which increases the length of the average diffusion path for a penetrant molecule. This effect can be expressed by

$$D = \kappa D^* \tag{6}$$

where D^* is the diffusion coefficient in the purely amorphous polymer ($\alpha = 1$) and κ is a structural factor which represents the degree of blocking

or impedance imposed on gas diffusion by the impermeable crystalline phase. Lasoski and Cobbs[2] established that for low to moderate levels of crystallinity, and when the crystalline phase is isotropically distributed in the polymer, the structural factor can be adequately represented as the amorphous volume fraction α thus:

$$D \cong D^*\alpha \tag{7}$$

Combining eqs. (3), (4), and (6), one obtains the permeability expression

$$P = \alpha k^* \kappa D^* = \alpha \kappa P^* \tag{8}$$

or, by using eq. (7) instead of (6),

$$P = \alpha^2 k^* D^* = \alpha^2 P^* \tag{9}$$

Equations (3), (7), and (9) can be utilized for comparing the sorption and transport properties of films having different crystallinities. This is done by correcting for the crystallinity effects with the factors α or α^2. Hence the quantities D/α and P/α^2 represent normalized transport properties that approximately eliminate the effect of crystallinity differences and more nearly represent the intrinsic transport behavior of the amorphous phase where transport occurs.

The effect of a processing operation, such as drawing or heat treatment, can be analyzed more generally by examining the changes in α and κ in eq. (8) upon such treatment. It must be noted that eq. (8) is oversimplified as it does not account for changes in the transport properties of the amorphous phase that can be induced by orientation or thermal treatment. The most important possibility is an immobilization of the rubbery chain segments imposed by the crystalline regions. This effect can be accounted for, following the treatment of Michaels and co-workers,[3,4] by use of an immobilization constant β that represents the degree of tautness in the intercrystalline rubbery segments. An increase in β is normally accompanied by an increase in the diffusion activation energy. The most general expression for P, thus, becomes

$$P = \alpha k^* D^* \kappa / \beta \tag{10}$$

Changes in permeability of PVF_2 to various gases following uniaxial drawing and/or heat treatment have been interpreted in terms of the changes occurring in α, κ, and β following such treatments.

Since molecular orientation induced by drawing was performed both in the melt state and below T_m, it is useful to begin by considering the mechanism for each of the two processes, and the physical properties and crystalline morphologies associated with each. Over the past two decades, considerable work has been done to elucidate the crystalline morphologies resulting from melt or solution crystallization under an applied strain.[5-15] Depending on the level of stress in the melt during crystallization, it is generally agreed that the crystalline microstructure will assume one of the first three morphologies depicted in Figures 1(a), (b), or (c). In the absence

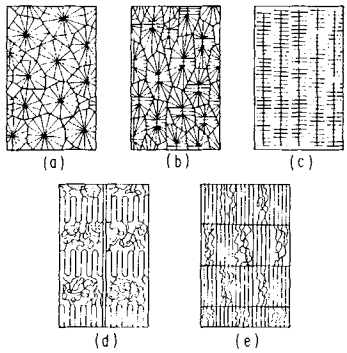

Fig. 1. Crystalline morphologies of semicrystalline polymers for different processing conditions: (a) crystallized form a quiescent melt (spherulitic structures); (b) crystallized under low stress (oriented spherulites); (c) crystallized under high stress (row structures); (d) detailed view of (c); (e) cold-drawn (microfibrillar structures).

of any stress, the crystallites grow into well-known spherulitic structures, forming a polygonal array, as schematically depicted in Figure 1(a). As strain is imposed on the crystallizing melt, the nucleating zones in the melt become progressively more elongated thin fibers, which allow crystalline lamellar growth to occur preferentially perpendicular to the direction of strain.[5-15] At very high strains, this results in complete replacement of the spherulitic morphology by a unidirectional morphology of row structures, sometimes referred to as a "shish kebab" morphology [Figs. 1(c) and 1(d)]. It consists, in the ideal case, of parallel lamellar platelets, separated by layers of interlamellar rubbery segments. For low and moderate strains, a gradual transition region between the two regimes exists, sketched in Figure 1(b), in which elongated spherulites possessing features common to the two limiting cases are present.

Orientation induced by drawing below the melting point must be of a fundamentally different nature from that described above. Instead of *crystallizing* the polymer under strain, this process involves a *morphological transformation* of existing crystalline structures. If the drawing temperature is 50°C or more below the melting point, necking occurs at an early stage of drawing. The necking process marks the onset of a transition stage, wherein the original spherulitic or microspherulitic structures are partially transformed into a fibrillar morphology consisting of alternating crystalline and amorphous bundles, with the drawn crystalline structures possessing a high degree of order along the chain axis.[16-19] An idealized picture of this morphology is depicted in Figure 1(e). As the draw ratio is increased beyond the fully developed neck, the fraction of the fibrillar morphology progressively increases.

The morphologies represented in Figure 1, which are a direct consequence of the processing steps performed, are believed to be a deciding factor in the gas transport behavior of the polymer, as is demonstrated in subsequent sections. Of particular interest is the essentially opposite morphological influences on gas transport produced by the high drawing above T_m vis-à-vis that well below T_m, which are embodied in Figures 1(d) and 1(e), respectively.

EXPERIMENTAL

Kynar PVF_2 film was obtained in extruded form from the Pennwalt Corp. The film had a nominal thickness of 6 mils and was slightly birefringent ($\Delta \sim 5 \times 10^{-3}$). Its density was 1.763 g/cc, and the crystallinity was 54% by weight as determined by DSC, based on a heat of fusion of 23.5 cal/g for the pure crystals.[20] The crystallinity value based on the film density was 52% using the volumetric data of Nakagawa and Ishida.[21] The calorimetric crystallinity estimates for various films were the ones utilized for comparisons and calculations.

Gases used in this study were He, Ar, N_2, CH_4, and CO_2. In addition to these five gases, H_2 and O_2 were also used to obtain transport properties for the untreated PVF_2. All gases had a purity of 99.8% or better except for CH_4 which was 99% pure.

The procedure employed for sample preparation is very similar to that described previously.[1] Briefly, rectangular strips of PVF_2 were clamped firmly in T-shaped grips, which were then mounted onto the crosshead mechanism of a table model Instron tester fitted with an environmental chamber. Drawing was performed at temperatures ranging from 75 to 140°C at a strain rate of 100% min^{-1}. These temperatures lie well above the glass transition temperature for PVF_2, which is about −40°C.

In order to isolate the effects of orientation from those of the accompanying thermal treatment, undrawn samples were exposed to the same drawing temperatures for the same duration as the drawn samples. Such samples are designated in our notation as having a draw ratio λ of 1.0 (or 1.0X) as opposed to the "as-received" film which underwent no such treatment.

Samples for permeation and physical characterization measurements of drawn film were, in every case, taken from the central portion of the drawn sample. Equilibrium gas sorption and transient permeation measurements were performed at 35°C using equipment described elsewhere.[22,23] The sample size used for the equilibrium sorption measurements was 5 cm^3 of polymer and the pressure range was 0–25 atm, except for CO_2, whose sorption was measured up to about 12 atm. Permeation runs, from which both the permeability and the diffusion time lag were obtained, were performed at 1–3 atm for He, H_2, and O_2; 20 atm for Ar, N_2, and CH_4; and at 1–20 atm for CO_2.

Density measurements for the as-received and treated samples were performed at 30°C in a Techne density gradient column using aqueous zinc chloride solutions and factory-calibrated glass floats. Measurement accuracy was to within ± 0.0002 g/cc. The total film birefringence Δ was measured by a Gaertner interferometer, utilizing polarized light and a Babinet compensator. A Perkin-Elmer DSC-II differential scanning calorimeter was used to study the melting behavior and determine the heats of fusion for PVF_2 samples used in this study. Data acquisition, calculations, and graphics were performed digitally by a Perkin-Elmer 3500 Thermal Analysis Data Station that was interfaced with the calorimeter. All the DSC thermograms of PVF_2 have been normalized to a unit-mass basis for comparison. A Rheovibron dynamic mechanical tester with automated control and digital data acquisition was used to characterize the dynamic mechanical behavior of

the PVF_2 film in the temperature range −120–120°C at a frequency of 110 Hz.

RESULTS AND DISCUSSION

Commercial Film

The sorption isotherms for N_2, Ar, CH_4, and CO_2 in the untreated, "as-received" commercial PVF_2 film are shown in Figure 2. The isotherms are linear as expected and the solubility coefficients k along with their transient counterparts k_t are given in Table I. Along with k and k_t, the corresponding amorphous phase solubility coefficients k^* and k_t^* defined in eq. (3) are also given. Helium sorption was too small to measure accurately by the equilibrium method. The solubilities of H_2 and O_2 were also obtained by the transient method.

Given the margin of error associated with sorption measurements, the agreement between the k and k_t values can be considered to be remarkable. As noted for numerous other polymers,[1,24–28] there is a linear correlation (represented by Fig. 3) between the logarithm of solubility and the Lennard–Jones potential well depth, ϵ/k for the gas.[29] This is true for both k and k_t, and the slopes are essentially identical being 6.5×10^{-3} and 6.7×10^{-3} K^{-1} for k^* and k_t^*, respectively. The solubility coefficient for CO_2 is about six times larger than predicted by the correlation line. Other polymers[1,30,31] which apparently exhibit specific interactions with CO_2 show similar behavior. Since CO_2 sorption in polyethylene[24] has been found to follow the correlation with the Lennard–Jones potential well depth closely, along with other gases, it seems that the high CO_2 solubility in PVF_2 can be ascribed to the polar nature of the PVF_2 repeating unit, which gives this polymer its propensity for attractive interactions with CO_2. This CO_2 sorption phenomenon at least partly explains the observations of Kiplin-

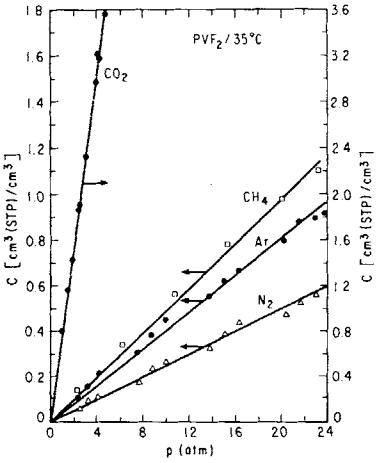

Fig. 2. Sorption isotherms for N_2, Ar, CH_4 and CO_2 in PVF_2 at 35°C.

TABLE I
Solubility Coefficients for Various Gases in As-Received Commercial PVF_2 Film at 35°C

Gas	ϵ/K (K)	k^a	k_t^a	k^{*a}	k_t^{*a}
He	10.2	—	0.0070	—	0.0142
H_2	38.0	—	0.0122	—	0.0248
N_2	91.5	0.0237	0.0237	0.0484	0.0484
O_2	113	—	0.0366	—	0.0747
Ar	124	0.0399	0.0409	0.0814	0.0835
CH_4	137	0.0463	0.0517	0.0945	0.105
CO_2	190	0.7304	0.694	1.491	1.414

[a] Units: cm^3 (STP)/cm^3 atm.

ger,[32] where surface fluorination of low density polyethylene markedly increased the CO_2 permeability relative to that of CH_4.

The transport properties for various gases in the untreated PVF_2 are summarized in Table II. In Figure 4, the diffusion coefficient D is correlated with the molecular diameter for seven gases: He, H_2, Ar, O_2, N_2, CH_4, and CO_2. The molecular diameter used for the correlation was the Lennard–Jones mean diameter of the gas deduced from viscosity measurements.[29] It was found that the diffusion coefficients for the linear molecules H_2, O_2, N_2, and Co_2 fall consistently above the correlation line drawn for the spherical molecules He, Ar, and CH_4. Linear penetrants are believed to accomplish most of their diffusional jumps with the long axis of the penetrant molecule oriented along the diffusion path—thus reducing the effective diameter in comparison to the average molecular diameter. The two curves in Figure 4 roughly constitute an "envelope" within which diffusion coefficients for other penetrants should fall. The expected position of D for a given penetrant between the two curves of Figure 4 should be largely dictated by penetrant shape. The diffusion coefficient for linear penetrants

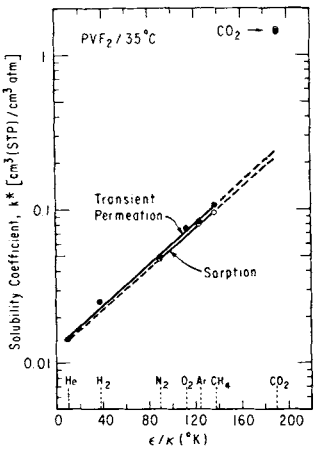

Fig. 3. Henry's law solubility coefficients obtained from equilibrium sorption and transient permeation plotted against the Lennard–Jones parameter, ϵ/k.

TABLE II
Permeability and Diffusion Coefficients for Various Gases in As-Received PVF_2 at 35°C

Gas	d (Å)	D^a	D^{*a}	P^b	P^{*b}
He	2.58	1.87×10^{-6}	3.81×10^{-6}	1.72×10^{-10}	7.16×10^{-10}
H_2	2.97	3.36×10^{-7}	6.86×10^{-7}	5.38×10^{-11}	2.24×10^{-10}
Ar	3.44	9.85×10^{-9}	2.01×10^{-8}	5.30×10^{-12}	2.21×10^{-11}
O_2	3.49	1.72×10^{-8}	3.50×10^{-8}	8.26×10^{-12}	3.44×10^{-11}
N_2	3.72	7.16×10^{-9}	1.46×10^{-8}	2.23×10^{-12}	9.30×10^{-12}
CH_4	3.84	2.94×10^{-9}	6.00×10^{-9}	2.00×10^{-12}	8.33×10^{-12}
CO_2[c]	3.95	5.66×10^{-9}	1.15×10^{-8}	5.17×10^{-11}	2.15×10^{-10}

[a] Units: cm^2/s.
[b] Units: cm^3 (STP) cm/cm^2 s cm Hg
[c] At 1 atm driving pressure; for other gases D was independent of pressure.

was found to be about twice that of spherical penetrants of the same mean molecular diameter.

Figures 3 and 4 provide the necessary correlations to predict the permeability of a given gas in PVF_2 at 35°C. The Lennard–Jones parameters ϵ/k and σ (the gas diameter) define k_t and D, whose produce is P. The solubility correlation, however, is not valid for gases which have favorable specific interactions with the material, such as CO_2. It should be noted that CO_2 plasticizes the polymer leading to a concentration dependent diffusion coefficient, and the value in Figure 4 corresponds to the low concentration limit.

Effect of Film Preparation Process

The gas transport properties for PVF_2 are affected by the physical process by which the film was prepared. While this is not the main thrust of this paper, it is useful to present a general picture of how the crystalline mor-

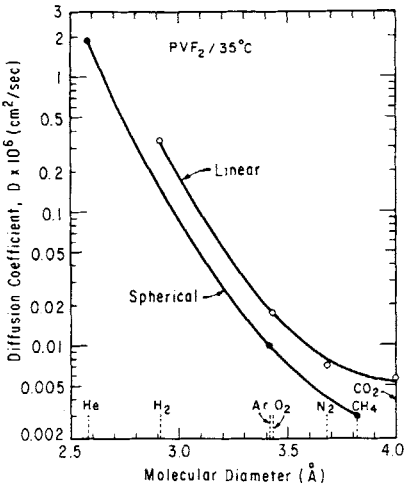

Fig. 4. Diffusion coefficients for various gases in PVF_2 at 35°C plotted against the Lennard–Jones collision diameter of the penetrant gas.

phology, which is a consequence of the crystallization and melt-processing history, influences gas transport in a semicrystalline polymer. To this end, we compared the He, Ar, and CH_4 permeabilities in the Kynar commercial PVF_2 film with those of four other films of the same material which were prepared by different processes. Some properties of these films are listed in Table III. In addition to the commercial film (designated as C in Table III), films D and E were made by melt extrusion in our laboratory, film A was prepared by spin-casting from solution, and film B was compression melt-pressed from C and cooled at a rate of ~40°C/min. The permeabilities for all three gases, curiously, seem to follow an increasing trend with birefringence as depicted graphically in Figure 5. The diffusion coefficient follows a similar trend as seen in Figure 6. The plots for the transport parameters are represented in two ways. The upper plots (a) of Figures 5 and 6 show the measured permeability and diffusion coefficients for PVF_2 directly plotted against Δ. The crystallinities of the extruded films (D and E) were somewhat lower than for the other films, as indicated in Table III, which partly accounts for a higher permeability in these films. In order to approximately remove this crystallinity effect, the transport parameters were scaled by the amorphous volume fraction by taking the ratios P/α^2 and D/α as described earlier. These quantities are plotted in the lower graphs, (b), of Figures 5 and 6, which demonstrate that higher differences in crystallinity cannot explain the almost twofold higher permeability for the melt extruded film with the highest birefringence relative to the spin-cast film with zero birefringence.

The transport results of Figures 5 and 6 can be understood in terms of the amount of hindrance imposed by crystallites on the diffusing species. From the arrangement of the crystalline lamellae for cases (a), (b), and (c) of Figure 1, it is obvious that the row-nucleated morphology should offer the lowest resistance to gas diffusion in the direction normal to the plane of the film. This is because the lamellae, being essentially impermeable barriers, are stacked so as to afford paths of virtually unhindered interlamellar rubbery channels for gas transport. The case of a quiescent (unstrained) melt, on the other hand, yields a nearly uniform distribution of lamellar orientations within spherulites, allowing the largest possible number of lamellae to assume orientations in the plane of the film, and thereby impeding gas transport.

The spin-cast and the compression-molded PVF_2 (samples A and B) can be adequately described as a having the morphology of Figure 1(a), and

TABLE III
Properties of PVF_2 Films from Different Processes

Film	Process	Thickness (mils)	Birefringence ($\times 10^3$)	Crystallinity (wt %)	α[a]
A	Spin casting	4.94	0.0	56	0.47
B	Compression molding	5.71	0.0	55	0.48
C	Extrusion-commercial	5.71	4.5	54	0.49
D	Extrusion-bench scale	7.00	10.9	46	0.57
E	Extrusion-bench scale	2.95	12.6	46	0.57

[a] α = amorphous volume fraction.

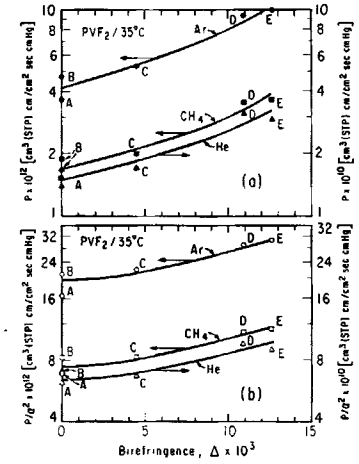

Fig. 5. Permeabilities of He, Ar, and CH_4 in PVF_2 at 35°C for films prepared by different processes plotted against film birefringence: (a) observed permeabilities; (b) permeabilities scaled to constant amorphous content by factor α^2. Preparation methods are given in Table III.

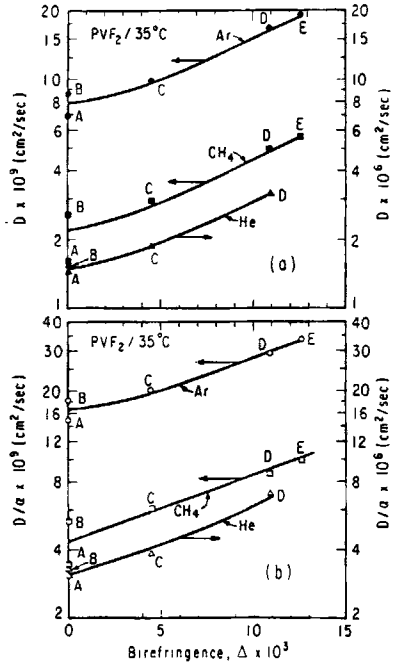

Fig. 6. Diffusion coefficients for He, Ar, and CH_4 in PVF_2 at 35°C for films prepared by different processes plotted vs. film birefringence: (a) observed diffusion coefficients; (b) diffusion coefficients scaled to constant amorphous content by factor α. Preparation methods are given in Table III.

hence must have the highest barrier characteristics based on the mechanistic picture presented above—which is indeed the case. The commercially and the bench-scale extruded films (C, D, and E), on the other hand, were subjected to stress during crystallization, and therefore possess morphologies that are akin to that of Figure 1(b). It is worth noting that films B and C have essentially the same transport properties, which indicates that the morphology of the commercial film is much more similar to the ordinary spherulitic type of Figure 1(a) than it is to the row-structure morphology of Figure 1(c).

Effect of Draw Ratio

The drawing behavior of PVF_2 below the melting point was found to follow one of two regimes, depending on the drawing temperature. At temperatures far removed from T_m (< 90°C), orientation proceeded via a necking mechanism followed by uniform deformation after complete conversion of the film to the necked state. For drawing temperatures close to T_m (> 110°C), uniform sample elongation was observed throughout the drawing process. The range (90–110°C) constituted a gradual transition region between the two temperature regimes. Under our conditions, the maximum attainable draw was essentially the same (~3.7) regardless of the drawing temperature.

In order to assess the effect of draw ratio on the transport properties of PVF_2, the intermediate temperature of 100°C was selected as the drawing temperature. On the other hand, the effect of drawing temperature was monitored by following changes in the transport behavior for a constant draw ratio of 3.7 over a temperature range from 75 to 140°C. The accompanying changes in optical, calorimetric, volumetric, and dynamic mechanical behavior were also analyzed.

The effect of draw ratio on the birefringence Δ of PVF_2 is shown in Figure 7. The point at $\lambda = 1.0$ represents a sample that was only heat-treated at 100°C for the same duration as the drawn samples. The small birefringence originally present in the as-received film did not change as a result of the heat treatment. The birefringence curve is of the pseudo-affine type, char-

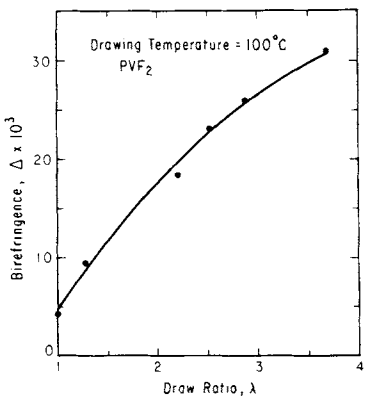

Fig. 7. Birefringence versus draw ratio for PVF_2 film drawn at 100°C.

acteristic of orientation behavior for semi-crystalline polymers.[33] The observed birefringence Δ is comprised of crystalline and amorphous contributions, but no attempt was made to resolve the birefringence into these constitutent contributions. Draw ratios in the range 1.3–2.3 could not be achieved due to the necking process which caused a step-change in the draw ratio within a restricted region of the sample. Sorption and transport studies were limited to drawn samples in which the strain was spread uniformly over the film surface. At 100°C, films with uniform draw could be achieved for draw ratios of 2.3 or higher. In the low strain region (up to $\lambda = 1.3$) uniform deformation was also observed prior to the formation of a necking zone. The effect of draw ratio on PVF_2 permeability to He, Ar, N_2, and CH_4 is shown in Figure 8. To facilitate comparison, the data are presented as a relative permeability, P/P_0, where P_0 is the permeability of the as-received film (see Table II). Again, a draw ratio of 1.0 denotes an undrawn sample with the same heating history as the drawn films. For Ar, N_2, and CH_4, P/P_0 declines sharply with λ for the initial stages of drawing, but starts to level off for $\lambda > 3.0$. He, on the other hand, shows only a very small (~10%) decline over the entire range of draw ratios. The extent of reduction in P/P_0 is greatest for CH_4 and seems to follow a trend related to penetrant size, i.e., $CH_4 > N_2 > Ar > He$. The data for CO_2 are also consistent with this trend as will be shown in a subsequent section. Another interesting feature of Figure 8 is the increase in P/P_0 for the heat-treated sample ($\lambda = 1.0$). This contradicts the intuitive expectation of a lower permeability as a result of increased order or crystallinity. An explanation for this behavior is also given later.

The reduction in permeability for the drawn film can be resolved into the independent changes in the diffusion and solubility components of P as shown in Figures 9 and 10. For these quantities, the results have also been normalized with respect to the "as-received" diffusion, D_0, and solu-

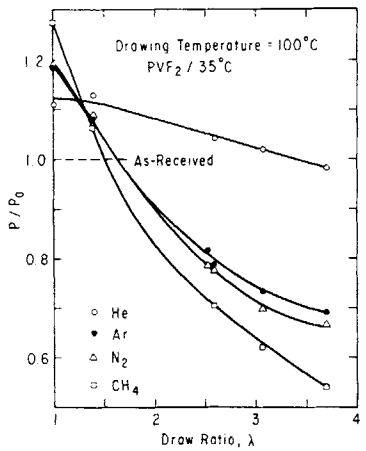

Fig. 8. Permeability , relative to "as-received" value, P_0, at 35°C for He (○), Ar (●), N_2 (△), and CH_4 (□) in PVF_2 as a function of draw ratio. (Drawing temperature = 100°C.) P_0 values are tabulated in Table II.

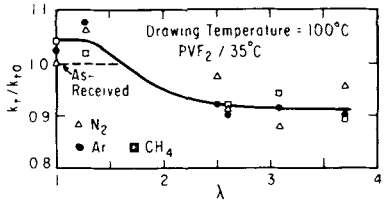

Fig. 9. Relative solubility, k_t/k_{t0}, derived from transient permeation as a function of draw ratio for N_2 (△), Ar (●), and CH_4 (□) in PVF_2 at 35°C. (Drawing temperature = 100°C.) k_{t0} values are shown in Table I.

bility, k_{t0}, coefficients. The solubility plotted in Figure 9 is that derived from the transient time-lag experiment. Figure 9 shows that the solubility drops by only about 10% as a result of drawing at 100°C. This reduction seems to be unchanged for $\lambda \geq 2.5$, or when the necking process is fully developed. Within experimental error, the reduction in solubility upon drawing is independent of the type of gas. The D/D_0 response to drawing (Fig. 10) on the other hand, closely follows that of permeability, exhibiting a steep slope at low draw ratios, then tapering off for higher λ. It also exhibits the same molecular size dependence as that of P/P_0. D/D_0 values for He are not reported because the time lags were too short to measure for drawn film. Figures 11 and 12 show P/P_0 and D/D_0 for each gas plotted against birefringence. In addition to being somewhat more linear than the responses shown in Figures 8 and 10, these plots serve as a reminder of the orientation which existed in the as-received film.

The effects of drawing at 100°C on the melting behavior for PVF_2 are shown in Figures 13 and 14. The slight reduction in the heat of fusion, ΔH_f, on drawing amounts to about 2–3% reduction in crystallinity if it is assumed that the heat of fusion for the 100% crystalline polymer is unchanged by drawing. This small reduction in ΔH_f may, however, be mostly due to the crystalline phase conversion for PVF_2 from form II to the less stable form I, which has been noted to have a higher internal energy relative to that of form II.[34] Also, the solubility results of Figure 9 do not support any

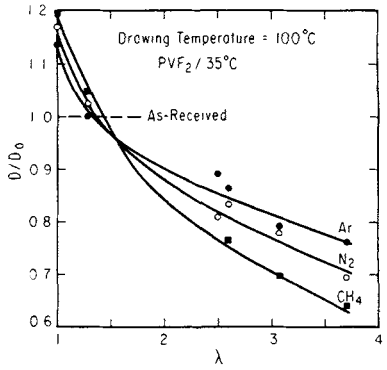

Fig. 10. Relative diffusion coefficients, D/D_0, as a function of draw ratio for N_2, Ar, and CH_4 in PVF_2 at 35°C. (Drawing temperature = 100°C.) D_0 values are given in Table II.

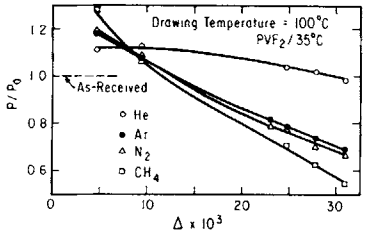

Fig. 11. P/P_0 as function of film birefringence for data of Figure 10: (○) He; (●) Ar; (△) N_2; (□) CH_4.

significant reduction in crystallinity since k must increase if this were the case, assuming the solubility coefficient for the amorphous phase is unchanged.

The conversion of the crystalline PVF_2 component from form II to form I has been the subject of many studies.[35-42] This crystalline transformation has been linked to important changes in the electrical behavior of PVF_2, but we believe it should, per se, have little influence on gas transport since the crystalline component should be impermeable to gases regardless of the molecular organization of the crystalline lattice. In Figure 14 the melting endotherm for a drawn PVF_2 sample ($\lambda = 3.7$) is shown superimposed on that of an undrawn sample with the same heating history ($\lambda = 1.0$). Drawing broadens the melting peak, reduces its height, and shifts the maximum to a higher temperature (by about 5°C). Another feature of the 3.7X endotherm is the absence of the annealing shoulder at around 100°C seen for the 1X sample. This is also the case for other drawing temperatures. The broadening of the melting peak is indicative of a broader distribution of crystallite sizes as a result of spherulitic and lamellar fragmentation and fibrillar growth. The disappearance of the annealing shoulder is probably due to the melting and reorganization of the originally thin lamellar sections into fibrous crystalline bundles possessing a long chain axis dimension. This shifts the melting point to higher temperatures. The effect of annealing the PVF_2 film at 100°C on the endotherm is also shown in Figure 14. This thermal treatment increased the height of the melting peak while narrowing the peak width (opposite to the effect of drawing), suggesting a narrower distribution of crystallite sizes.

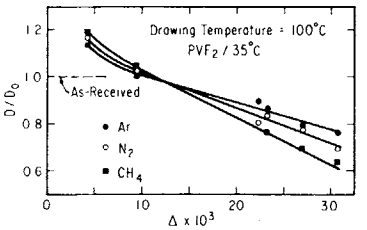

Fig. 12. D/D_0 as function of film birefringence for data of Figure 10: (●) Ar; (○) N_2; (■) CH_4.

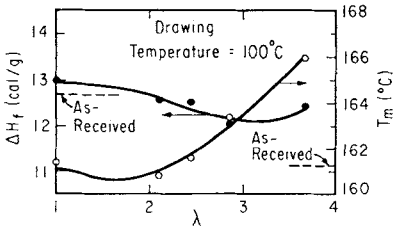

Fig. 13. Heat of fusion and melting point of PVF_2 as a function of draw ratio. (Drawing temperature = 100°C.)

The effect of PVF_2 drawing on the density of the polymer is shown in Figure 15. The density exhibits a modest increase at high draw ratios for a drawing temperature of 100°C. This increase agrees in general with the findings of Shuford et al.,[42] but differs in the shape of the curve for density v. λ. In Shufford's study the density increased more abruptly in the low λ region, leveling off at high λ, whereas in this study we noted an initial dip in the density below the as-received level for low draw ratios which eventually swings upward with λ in an essentially monotonic fashion beyond the point at which the necking zone is fully developed (λ > 2.5). Our density result agrees with the recent work of Wang and Porter[43] on cold-drawn polyethylene film, in which a similar density response to drawing is believed to have taken place accompanying the PE crystallinity which declines over the range of draw ratios of 1–2.5 and increases for λ > 2.5. In conjunction with the thermal analysis results presented here, however, the density

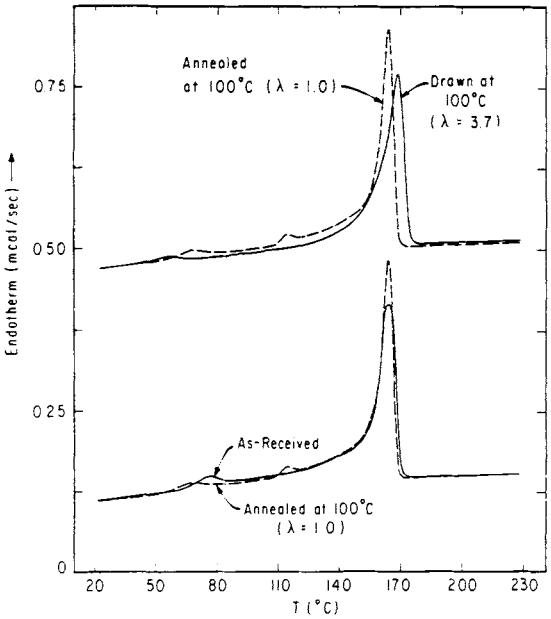

Fig. 14. Melting endotherms for as-received, annealed, and drawn PVF_2. (Annealing and drawing temperature = 100°C.)

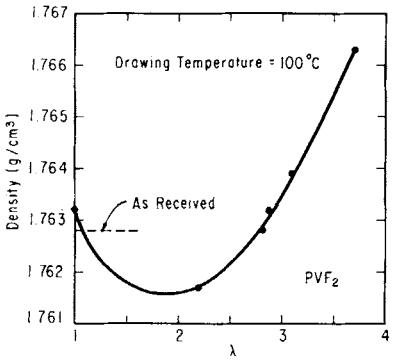

Fig. 15. Density of PVF_2 as a function of draw ratio. (Drawing temperature = 100°C.)

increase cannot be due to a higher crystalline fraction, but can be reasonably attributed to the increased fraction of the form I crystal, which has a higher density than that of form II.[34,44] The rise in density might also be construed, in part, as a densification in the rubbery phase on drawing. Hence, the observed reductions in P and D cannot be attributed to any significant increase in crystallinity.

Deforming a semicrystalline polymer below the melting point, in the necking and post-necking stages, involves a transformation in the superstructure of the crystalline lamellae. The original spherulitic or microspherulitic structures are gradually transformed into a microfibrillar morphology consisting of alternating crystalline and taut tie amorphous segments.[16-19] The tautness of the tie segments usually alters the physical character of these regions substantially, with a concommitant reduction in their transport properties. The change in these microfibrillar amorphous regions is believed to render these segments less mobile forming, together with the rest of the microfibril, a more impermeable barrier. This has been established from a number of studies, mostly involving the transport of organic vapors[45-48] in polyethylene. This morphological change forces a diffusing penetrant to circumvent the microfibrils, increasing the length of the mean diffusion path.

The changes in tortuosity are not expected to be identical for all gases. Helium, with a small molecular diameter, can more easily follow short alternate diffusion passages around the microfibrils than can larger penetrants like CH_4. This explains the observed dependence of the drawing response for the diffusion coefficient on the molecular size of the penetrant. The incorporation of a small fraction of the amorphous phase into the inactivated fibrillar state reduces slightly the effective amorphous fraction, thereby lowering the solubility k_t for the drawn material as depicted in Figure 9. The solubility result of Figure 9 supports the notion of a transformation in the polymer at necking which reduces the effective amorphous fraction; this is evidenced by the fact that the value of k_t drops abruptly for $\lambda = 2.5$ and remains essentially unchanged for higher λ. At $\lambda = 3.7$, the transformation to the fibrillar state is probably far from being complete and, hence, the effective amorphous volume fraction is only slightly reduced

and the tortuosity does not dramatically increase.[49] The above transport results are in good agreement with those reported by Yasuda and Peterlin[49] on the transport of CO_2 in drawn low-density polyethylene.

The role of the amorphous phase in the orientation behavior of PVF_2 can be inferred from the dynamic mechanical testing results of Figure 16. The loss tangent curve for the drawn sample ($\lambda = 3.7$) shows a broader and lower peak, indicative of a weaker transition, which is shifted to a slightly higher temperature. This mechanical transition behavior corresponds to the immobilization or tautness of the rubbery tie segments restrained within the microfibril elements. The shift in the broad transition from 55 to 110°C is associated with the transformation in the crystalline component from phase II to phase I as determined from the study of Kakutani.[50] In the following section, these dynamic mechanical transitions are also used to elucidate the effect of drawing temperature on the morphology and transport properties of drawn PVF_2.

The increase in P and D on annealing PVF_2 at 100°C may be the result of two contributing factors. While annealing below T_m is not sufficient to remove the orientation in the original film (as was verified from birefringence measurements), it can impart mobility to some of the taut amorphous interlamellar segments, thereby reducing the elastically ineffective amorphous fraction, which causes a net reduction in the immobilization parameter β. The other possible influence is the partial melting and recrystallization during the annealing cycle, which can enhance the character of the row-nucleated structures in the overall crystalline morphology. That, in turn, enhances gas transport as discussed earlier. Roughly the same increase in P was observed upon annealing a drawn sample ($\lambda = 3.7$) for 1 h at constant strain, immediately following drawing. Annealing the spin-cast sample designed by A in Table III did not produce an effect as significant as that for the commercial film but an increase was still discernible. These results are summarized in Table IV.

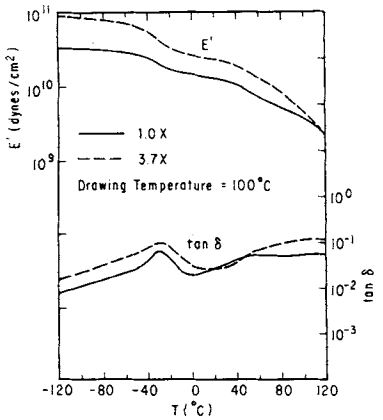

Fig. 16. Storage modulus E' and loss tangent, tan δ, for undrawn/annealed (1.0X) (—) and drawn (3.7X) (---) PVF_2. (Drawing temperature = 100°C; frequency = 110 Hz.)

TABLE IV
Effect of Annealing at 100°C on Gas Permeabilities of Different PVF_2 Films

Film	Treatment	$P \times 10^{10}$ [a] for He	$P \times 10^{12}$ [a] for Ar	$P \times 10^{12}$ [a] for CH_4
Spin-cast	Untreated	1.39	3.64	1.52
	Annealed at 100°C (1.0X)	1.44	3.94	1.83
Commercial	As-received	1.72	5.30	2.00
	Annealed at 100°C (1.0X)	1.91	6.35	2.48
Drawn Commercial	Drawn at 100°C (3.7X)	1.69	3.64	1.14
	Annealed at 100°C after drawing (3.7 X)	1.72	—	1.26

[a] Units as given in Table II.

The dynamic mechanical results of Figure 17 reveal a change in the low-temperature response of tan δ upon annealing. The lower tan δ and its greater dependence on temperature below the transition reflects changes in segmental mobility in the amorphous regions of the annealed sample consistent with the transport results.

To determine whether the effect of orientation below T_m is dependent on the original sample history, the permeability data for He, Ar, and CH_4 are compared in Table V for the commercial film, drawn along both the machine and transverse directions of the original film, with those of a PVF_2 film prepared by spin-casting. The ratios of the permeabilities for the drawn to the undrawn film are nearly the same for the commercial and the spin-cast materials, and the draw direction for the commercial film seems to have little effect on this quantity.

Since the reduction in P and D stems primarily from morphological or geometrical aspects of tortuosity, the activation energy for the diffusion process is not expected to change significantly. This is verified experimentally by the Arrhenius plots of Figures 18 and 19 for 1.0X and 3.0X samples

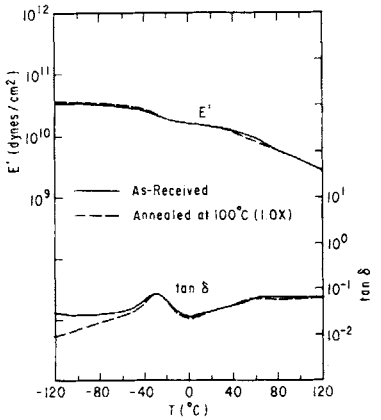

Fig. 17. E' and tan δ responses showing the effect of annealing as-received (—) PVF_2 at 100°C (1.0X) (---) (frequency = 110 Hz).

TABLE V
Comparison between Drawing Results of Spin-Cast Film with Those of Commercial Film Drawn along Two Directions

Film		$P^a \times 10^{10}$	$P \times 10^{12}$ [a]	$P \times 10^{12}$ [a]
Preparation	Drawing	for He	for Ar	for CH_4
Spin-casting	1.0X at 100°C	1.44	3.94	1.83
	3.7X at 100°C	1.26	2.66	0.88
Commercial	1.0X at 100°C	1.91	6.35	2.48
	3.7X at 100°C/MD[b]	1.69	3.64	1.14
	3.9X at 100°C/TD[c]	1.67	3.58	1.18

[a] Units as defined in Table II.
[b] Sample drawn along original machine direction.
[c] Sample drawn along original transverse direction.

drawn at 100°C. Figure 20 shows the accompanying solubility data. The Arrhenius parameters derived from these plots are listed in Table VI. The constant activation energy agrees with results for a dibutyl malaete copolymer by Michaels, Vieth, and Bixler[51] and our previous study involving PVC.[1]

Effect of Drawing Temperature

As stated earlier, the nature of the deformation process for PVF_2 depends on the drawing temperature. Some polymer properties are more affected by the drawing temperature than others. The film birefringence, for example, shows surprising constancy over the temperature range from 75 to 125°C and starts to decline appreciably only for drawing temperatures great-

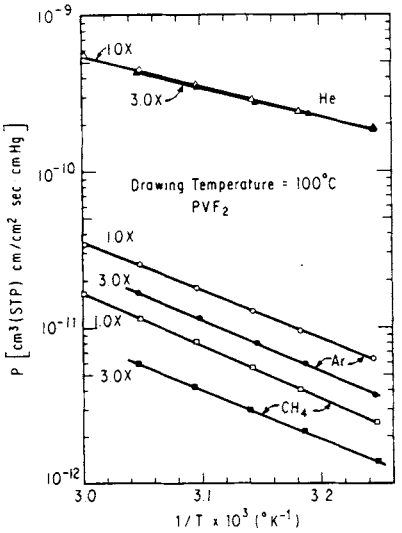

Fig. 18. Permeability of He, Ar, and CH_4 for annealed (1.0X) and drawn (3.0X) PVF_2 plotted in the Arrhenius form.

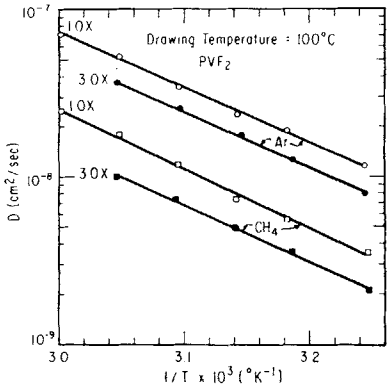

Fig. 19. Diffusion coefficients of Ar and CH_4 for annealed (1.0X) and drawn (3.0X) PVF_2 plotted in the Arrhenius form.

er than 140°C as shown in Figure 21. The heat of fusion is only slightly affected by orientation or the drawing temperature as shown in Figure 22. The shape of the melting endotherm changes slightly as the drawing temperature is raised attaining progressively greater height-to-width ratio of the peak as evident from Figure 23. This is in line with the interpretation of the peak flattening in terms of lamellar fragmentation and fibrillar structure formation upon necking.

The relative permeability, P/P_0, for He, Ar, and CH_4 is plotted against the drawing temperature in Figure 24. There is a monotonic decline in P/P_0 with decreasing drawing temperature, which levels off somewhat for temperatures below 90°C. For the 1.0X samples, P/P_0 is almost independent of the processing temperature between 75 and 125°C but increases slightly above 125°C. The corresponding responses for the diffusion and solubility

TABLE VI
Arrhenius Parameters for PVF_2 Drawn (3.0X) and Annealed (1.0X) at 100°C

Gas	Parameter[a]	1.0X	3.0X
He	E_p	8.595	8.60
	P_0	2.331	2.282
Ar	E_p	13.96	14.91
	P_0	4.992×10^{-2}	14.2×10^{-2}
	E_D	14.94	15.53
	D_0	457.7	819.5
	ΔH_s	-0.984	-0.605
	k_{s0}	8.27×10^{-2}	1.33×10^{-2}
CH_4	E_p	15.46	14.39
	P_0	0.2299	0.0225
	E_D	16.13	15.48
	D_0	950.3	208.8
	ΔH_s	-0.842	-1.088
	k_{s0}	1.41×10^{-2}	8.18×10^{-2}

[a] Units: E_p (kcal/g mol), P_0 (cm^3 (STP) cm/cm^2 s cm Hg), E_D (kcal/g mol), D_0 (cm^2/s), ΔH_s (kcal/g mol), and k_{s0} (cm^3 (STP)/cm^3 atm).

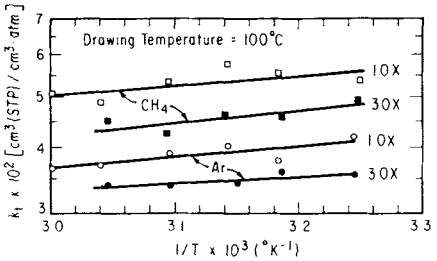

Fig. 20. Solubility of Ar and CH_4 for annealed (1.0X) and drawn (3.0X) PVF_2 plotted in the Arrhenius form.

coefficients are shown in Figures 25 and 26, respectively. Instead of mimicking the permeability response, the diffusion coefficient changes more continuously over the temperature range investigated. The solubility coefficient seems to exhibit a slight minimum versus drawing temperature.

In Figure 27, results for CO_2 permeability in PVF_2 are presented to show the effects of both the drawing temperature (at $\lambda = 3.7$) and CO_2 pressure. The permeability of CO_2 was found to be dependent on the CO_2 driving pressure and on the prior exposure history of the PVF_2 film to CO_2. In order to eliminate the latter effect, CO_2 permeability runs on each film were taken by starting at 1 atm and progressively increasing the driving pressure for following runs, up to the last at 20 atm. The dependence of CO_2 permeability on prior CO_2 exposure is similar to that observed for PVC.[1] Briefly, the conditioning effect can be described as follows. Exposure to high CO_2 pressures (e.g., 20 atm) causes the low pressure permeability to increase. This increase was found to gradually decay, however, over a period of several weeks, until the conditioning effect was almost completely erased. The data in Figure 27, therefore, describe the pressure dependence of CO_2 permeability in the absence of these conditioning effects. This dependence is adequately represented by a straight line for the pressure range from 1 to 20 atm. Similar behavior was observed over the same pressure range for high-density polyethylene[52]; but this was not the case for the CO_2 pressure dependence observed recently in some glassy polymers such as PMMA.[53] These exhibit a strongly nonlinear dependence on CO_2 pressure. The CO_2 pressure dependence reflects the propensity of the polymer to be plasticized as a result of CO_2 sorption, which raises the diffusion coefficient due to increased segmental mobility in the polymer.

The effect of drawing temperature on the CO_2 permeability of drawn PVF_2 agrees well with that observed for the other gases in Figure 24. The

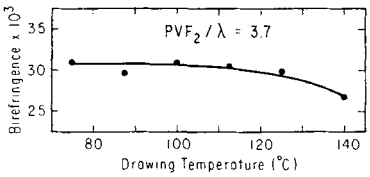

Fig. 21. Film birefringence versus the drawing temperature for PVF_2 drawn to 3.7X.

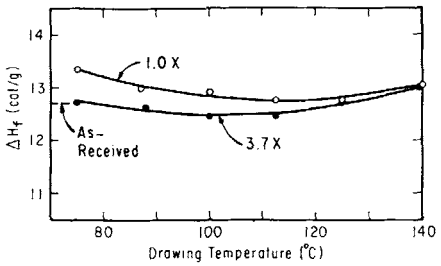

Fig. 22. Heat of fusion for PVF_2 drawn to 3.7X and 1.0X (annealed) vs. the drawing temperature.

state of orientation in the polymer had virtually no effect on the nature and magnitude of the CO_2 pressure dependence of P regardless of the drawing temperature. The small reduction in gas solubility noted for Ar, N_2, and CH_4 via the transient method (Figures 9 and 26) is supported by the equilibrium sorption data for drawn and undrawn CO_2 plotted in Figure 28. The solubility constants for the 3.7X film drawn at 100°C is about 12% below that of the as-received film (shown in Table I), and for the heat-treated sample, 1.0X, it is above the as-received value by about 8%, also in agreement with Figure 9. The net effect of drawing PVF_2 to $\lambda = 3.7$ on the CO_2 solubility is thus roughly a 20% decline in k.

The response of the permeability to drawing temperature, shown in Figures 24 and 27, can be explained on the basis of the effect that temperature has on the deformation process. As stated before, drawing in the neighborhood of T_m is expected to produce different microstructures from those at temperatures well below T_m. A number of studies in the literature report a similar role for the drawing temperature in connection with the phase transformation in PVF_2 from form II to form I.[37, 38, 40, 42] At low drawing temperatures, the sample deformed via the progressive spreading of a well-defined necking zone that forms at an early stage of the deformation process. A stress concentration is present in this necking region, and, as a result,

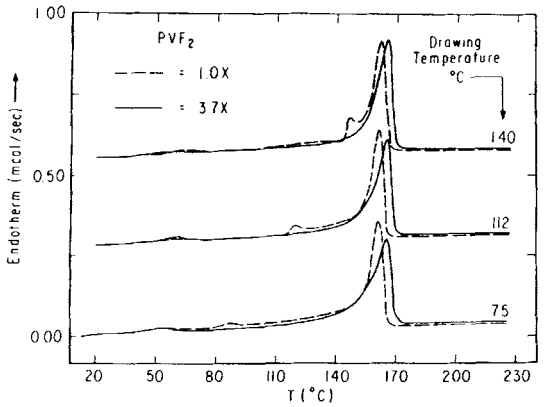

Fig. 23. Melting endotherms for PVF_2 films draw at three temperatures: (---) 1.0X; (—) 3.7X.

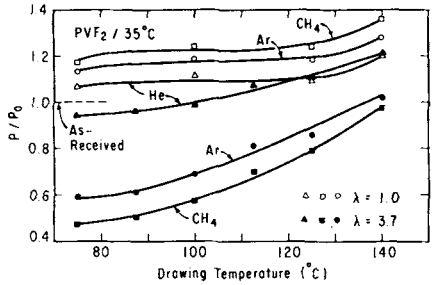

Fig. 24. Effect of the drawing temperature on P/P_0 for He, Ar, and CH_4 in PVF_2 at 35°C: (△, □, ○) λ = 1.0; (▲, ■, ●) λ = 3.7.

the spherulitic morphology is transformed into a microfibrillar morphology with an accompanying transformation in the crystalline component from phase II to phase I. This behavior is documented in a number of studies.[37,38,40,42] On the other hand, when the drawing temperature is well within the "tail" region of the melting endotherm, which begins at about 80°C, the mobility of the rubbery segments is greatly enhanced, and the amorphous fraction during drawing is increased due to the fusion of the low-melting crystals. Thus, the polymer matrix as a whole is capable of distributing the stress and accommodating more uniform deformation without neck formation. High stresses are, therefore, not attained at moderate draw ratios, and the fibrillation of the crystalline phase is severely restricted. As a side consequence, the II to I transformation in the crystalline matrix does not occur, since this phase change requires a minimum critical stress for it to be accomplished.[40,54] The effectiveness of drawing in transforming the PVF_2 morphology into a fibrillar type is believed to be enchanced as the drawing temperature is lowered. Consequently, P and D are reduced further accompanying the imminent tortuosity increases resulting from the enhancement of fibrillation.

As noted before, in the absence of other volumetric changes, the transformation in the PVF_2 crystalline component from phase II to I should entail an increase the density of the polymer. Thus, in connection with the role played by the drawing temperature in effecting this transformation, the densities of the drawn PVF_2 samples are expected to increase relative

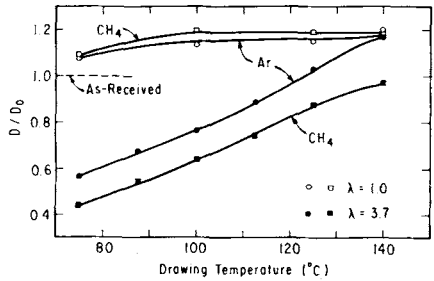

Fig. 25. Effect of the drawing temperature on D/D_0 for Ar and CH_4 in PVF_2 at 35°C: (○, □) λ = 1.0; (●), ■) λ = 3.7.

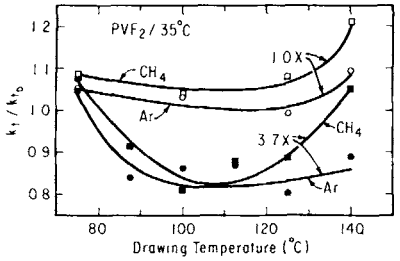

Fig. 26. Effect of the drawing temperature on k_t/k_{t0} for Ar and CH_4 in PVF_2 at 35°C.

to their undrawn (1.0X) counterparts with decreasing drawing temperature. With one exception, being the sample drawn at 75°C, the density data of Figure 29 do verify the role of the processing temperature discussed above, as the difference in density between the 3.7X and the 1.0X was found to become larger with decreasing temperature. The abrupt decrease in density for the sample drawn at 75°C is probably due to the superposition of the density increase caused by the II to I phase transformation and a density reduction due to possible microvoid formation or a slight reduction in crystallinity upon drawing, either of which would also explain the increased solubility in the 3.7X sample drawn at 75°C compared to films drawn at slightly higher temperatures (Fig. 26).

In terms of gas transport, the structural changes at low drawing temperatures translate into a greater tortuosity and, hence, a lower permeability compared to drawing at high temperatures. It must be emphasized that the increased barrier behavior is not at all due to the crystalline transformation from II to I, but rather both phenomena are results of fibrillation in the polymer. The dynamic mechanical results shown in Figure 30 illustrate the effect of the drawing temperature on the loss tangent response for films drawn at 75 and 125°C. The tan δ peak for the film drawn at 75°C is somewhat broader and is shifted to a higher temperature com-

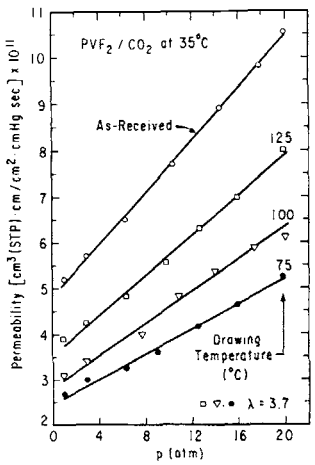

Fig. 27. CO_2 permeability as a function of upstream pressure for the as-received PVF_2 film and for films drawn at three temperatures ($\lambda = 3.7$) (□, ▽, ●).

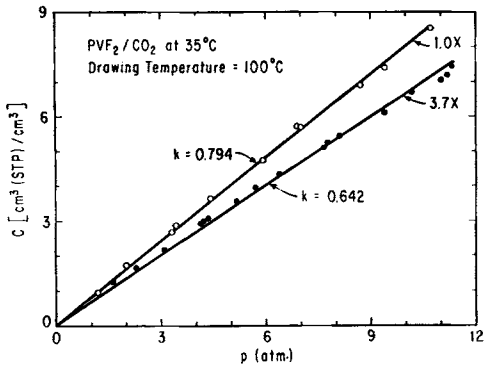

Fig. 28. CO_2 sorption isotherms at 35°C for PVF_2 films annealed (1.0X) and drawn (3.7X) at 100°C. The solubility coefficients k for both samples are given in $cm^3(STP)/cm^3$ atm.

pared to that of the film drawn at 125°C. This is due to the presence of taut intercrystalline rubbery elements incorporated in the microfibrils of the 75°C sample, which are absent in the 125°C sample. The weak broad transition above about 50°C is more pronounced for the 75°C sample than it is for the 125°C sample, indicating a higher degree of crystalline conversion from form II to form I in the former. The shape of this transition for the 125°C film is, in fact, more akin to those of the undrawn samples. One should note that the elastic moduli for the two samples remained essentially the same, which agrees with the findings of Richardson et al.[37] The Young's modulus is, thus, another quantity that is insensitive to processing temperature.

Finally, the reductions in permeability expressed by P/P_0 in Figures 8, 24, and 27 are correlated in Figure 31 with the Lennard–Jones molecular diameter of the gas. A straight line is fitted to the data for each of the three drawing temperatures 75, 100, and 125°C, and for the five gases He, Ar, N_2, CH_4, and CO_2. Figure 30 also manifests some shape (i.e., spherical vs. linear) effect on the ratios P/P_0 or D/D_0, as the P/P_0 for the linear molecules N_2 and CO_2 seemed to consistently fall above the correlation line, whereas the reverse was true for the cases of spherical penetrants, Ar and CH_4.

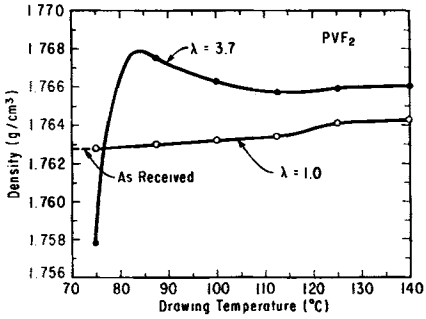

Fig. 29. Effect of drawing temperature on PVF_2 density for constant draw ratios of 1.0 and 3.7.

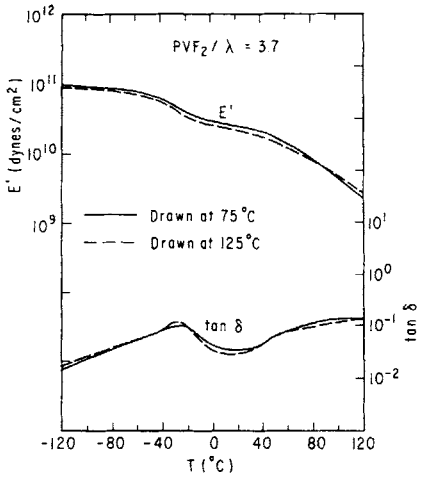

Fig. 30. Dynamic mechanical data for PVF_2 films drawn at 75 (—) and 125°C (---) ($\lambda = 3.7$).

CONCLUSIONS

This study elucidates a number of issues pertaining to the sorption and transport properties of gases in PVF_2 and the effects of orientation and processing variables on these properties.

The Henry's law sorption coefficients for fixed gases in PVF_2 can be correlated by the linear, semilogarithmic relation with the Lennard–Jones potential well depth of the gas known to hold for many polymers and liquids. The solubility of CO_2 is an exception to this, being about six times higher than predicted by the correlation. This behavior has been observed for CO_2 sorption in certain other polymers as well and has been attributed to specific interactions between CO_2 and the polymer repeating unit. The diffusion coefficients for various gases in PVF_2 correlate with the molecular diameter of the gas (up to 4.0 Å) by means of two curves, one for spherical and the other for linear penetrants, lying about twofold above the former.

Drawing PVF_2 at temperatures of 110°C or below alters the morphology of the crystalline structure visualized as breaking up the original spherulitic matrix into smaller lamellar aggregates to form a fibrillar morphology. This transformation causes significant reductions in the permeabilities of

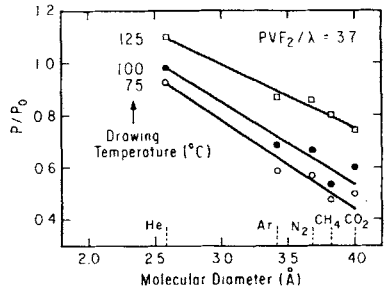

Fig. 31. Relative permeability, P/P_0, plotted as a function of the Lennard–Jones diameter of the gas for $\lambda = 3.7$.

Ar, N_2, CH_4, and CO_2, but only a slight decline (~10%) in that of He. The changes in permeability are caused by increased impedance to diffusion from the fibrillar elements and alteration of the amorphous state since the extent of the changes are a function of the molecular size of the penetrant. The degree of crystallinity remained essentially unaffected by orientation; however, films drawn at low temperature show evidence of a transformation in the crystalline phase from form II to form I. This transformation is accompanied by a more pronounced alpha transition by dynamic mechanical testing and, depending on the drawing temperature, by an increase in density. The reductions in permeability originated primarily from changes in the diffusion coefficient. Solubility, even though slightly (10–15%) reduced by orientation, was found relatively insensitive to processing treatments, in agreement with the small changes observed in free volume.

The effect of drawing on the permeability becomes more pronounced with decreasing drawing temperature then levels off around 75°C. This temperature dependence has been attributed to a greater conversion of the crystalline phase from the lamellar to the fibrillar morphology as the drawing temperature is lowered. Drawing at low temperatures (<90°C) occurred by necking at an early stage of deformation whereas a uniform deformation process was observed at temperatures greater than 110°C. Given the strong dependence of P and D on drawing temperature, these parameters can be more useful measures of the effectiveness of drawing in transforming the PVF_2 morphology in the manner described. The sensitivity of permeation to drawing temperature is, for example, much more than it is for birefringence or dynamic mechanical modulus.

Annealing PVF_2 film, regardless of the extent of orientation, at temperatures above 75°C was found to increase both P and D owing to increased mobility of the amorphous tie chains within the crystalline structures. The increase in P and D was very small for helium and became progressively more pronounced with increasing molecular diameter.

Gas transport results for PVF_2 films prepared by melt extrusion and other processes show that orientation introduced by straining the melt results in an increase in P and D as opposed to the decrease observed upon drawing below T_m. The origin of this behavior is hypothesized to lie in the crystallization process within a strained melt—namely row nucleation followed by epitaxial lamellar growth perpendicular to the direction of strain, which brings about a lower diffusional impedance. While this issue still calls for further investigation, the results as a whole shed light on the crucial role played by processing temperature on gas transport properties of a semicrystalline polymer.

This research was supported by the National Science Foundation through Grants DMR-80-01665 and CPE-83-06952.

References

1. M. J. El-Hibri and D. R. Paul, *J. Appl. Polym. Sci.*, **30**, 3649 (1985).
2. S. W. Lasoski and W. H. Cobbs, Jr., *J. Polym. Sci.*, **36**, 21 (1959).
3. A. S. Michaels and R. B. Parker, Jr., *J. Polym. Sci.*, **41**, 53 (1959).
4. A. S. Michaels and H. J. Bixler, *J. Polym. Sci.*, **40**, 413 (1959).
5. J. N. Hay, in *Flow-Induced Crystallization in Polymer Systems*, R. L. Miller, Ed., Gordon and Breach, New York, 1979, pp. 69–98.

6. A. Peterlin, in Ref. 5, pp. 1–29.
7. T. Kawai, M. Iguchi and H. Tonami, *Kolloid-Z.*, **221**, 28 (1967).
8. C. A. Garber and E. S. Clark, *J. Macromol. Sci. Phys.*, **B4**, 499 (1970).
9. A. Keller and M. J. Machin, *J. Macromol. Sci. Phys.*, **B1**, 41 (1967).
10. M. J. Hill and A. Keller, *J. Macromol. Sci. Phys.*, **B3**, 153 (1969).
11. R. B. Williamson and W. F. Busse, *J. Appl. Phys.*, **38**, 4187 (1967).
12. A. Peterlin, *Polym. Eng. Sci.*, **16**, 126 (1976).
13. V. G. Baranor and K. A. Gasparian, *Vysokomol. Soedin*, **All**, 809 (1969).
14. F. C. Frank, A. Keller and M. R. Mackley, *Polymer*, **12**, 467 (1971).
15. G. S. Y. Yeh, *Polym. Eng. Sci.*, **16**, 138, 145 (1976).
16. A. Peterlin, *J. Polym. Sci., C*, **9**, 61 (1965).
17. A. Peterlin, *Kolloid-Z.*, **233**, 857 (1969).
18. A. Peterlin, *Polym. Eng. Sci.*, **9**, 172 (1969).
19. A. Peterlin, *J. Mater. Sci.*, **6**, 490 (1971).
20. T. Nishi and T. T. Wang, *Macromolecules*, **8**, 909 (1975).
21. K. Nakagawa and Y. Ishida, *Kolloid-Z.*, **251**, 103 (1973).
22. W. J. Koros, D. R. Paul, and A. A. Rocha, *J. Polym. Sci., Polym. Phys. Ed.*, **14**, 687 (1976).
23. W. J. Koros, D. R. Paul, M. Fujii, H. B. Hopfenberg, and V. Stannett, *J. Appl. Polym. Sci.*, **21**, 2899 (1977).
24. A. S. Michaels and H. J. Bixler, *J. Polym. Sci.*, **50**, 393 (1961).
25. W. J. Koros, A. H. Chan, and D. R. Paul, *J. Membr. Sci.*, **2**, 165 (1977).
26. A. J. Erb and D. R. Paul, *J. Membr. Sci.*, **8**, 11 (1981).
27. P. Masi, D. R. Paul and J. W. Barlow, *J. Polym. Sci., Polym. Phys. Ed.*, **20**, 15 (1982).
28. K. Toi, G. Morel, and D. R. Paul, *J. Appl. Polym. Sci.*, **27**, 2997 (1982).
29. B. R. Bird, W. E. Stewart, and E. N. Lightfoot, *Transport Phenomena*, Wiley, New York, 1960, pp. 744–745.
30. J. S. Chiou and D. R. Paul, to appear.
31. W. J. Koros, paper presented at the AIChE Spring Meeting, Anaheim, CA, May 1984.
32. C. Kiplinger, M. S. thesis, University of Texas at Austin, 1983.
33. L. Holliday and I. M. Ward, in *Structure and Properties of Oriented Polymers*, I. M. Ward, Ed., Applied Science, London, 1975, Chap. 1.
34. R. Hasegawa, M. Kobayashi, and H. Tadokoro, *Polym. J.*, **3**, 591 (1972).
35. K. Yamada, M. Oie and M. Takayanagi, *J. Polym. Sci., Polym. Phys. Ed.*, **22**, 245 (1984).
36. J. B. Lando, H. G. Olf, and A. Peterlin, *J. Polym. Sci., A-1*, **4**, 941 (1966).
37. A. Richardson, P. S. Hope, and I. M. Ward, *J. Polym. Sci., Polym. Phys. Ed.*, **21**, 2525 (1983).
38. K. Yamada, M. Oie, and M. Takayanagi, *J. Polym. Sci., Polym. Phys. Ed.*, **21**, 1063 (1983).
39. W. T. Mead, A. E. Zachariades, T. Shimada, and R. S. Porter, *Marcomolecules*, **12**, 473 (1979).
40. B. P. Kosmynin, Y. L. Gal'perin, and D. Y. Tsvankin, *Vysokomol. Soyed.*, **A12**, 1254 (1970).
41. S. Enomoto, Y. Kawai, and M. Sugita, *J. Polym. Sci. A-1*, **6**, 861 (1968).
42. R. J. Shuford, A. F. Wilde, J. J. Ricca, and G. R. Thomas, *Polym. Eng. Sci.*, **16**, 25 (1976).
43. L. H. Wang and R. S. Porter, *J. Polym. Sci., Polym. Phys. Ed.*, **22**, 1645 (1984).
44. W. W. Doll and J. B. Lando, *J. Macromol. Sci. Phys.*, **B4**, 889 (1970).
45. L. Araimo, F. De Candia, V. Vittoria, and A. Peterlin, *J. Polym. Sci., Polym. Phys. Ed.*, **16**, 2087 (1978).
46. J. L. Williams and A. Peterlin, *J. Polym. Sci., A-2*, **9**, 1483 (1971).
47. A. Peterlin, J. L. Williams and V. Stannett, *J. Polym. Sci.*, A-2, **5**, 957 (1967).
48. A. Peterlin and J. L. Williams, *Br. Polym. J.*, **4**, 271 (1972).
49. H. Yasuda and A. Peterlin, *J. Appl. Polym. Sci.*, **18**, 531 (1974).
50. H. Kakutani, *J. Polym. Sci., A-2*, **8**, 1177 (1970).
51. A. S. Michaels, W. R. Vieth, and H. J. Bixler, *J. Appl. Polym. Sci.*, **8**, 2735 (1964).
52. M. J. El-Hibri, unpublished data.
53. J. S. Chiou and D. R. Paul, to appear.
54. J. C. McGrath and I. M. Ward, *Polymer*, **21**, 855 (91980).

Received August 13, 1985
Accepted October 5, 1985